The Astrophysical Journal, 866:105 (9pp), 2018 October 20 https://doi.org/10.3847/1538-4357/aade8d

Production of Mo and Ru Isotopes in Neutrino-driven Winds: Implications for Solar Abundances and Presolar Grains

J. Bliss[1], A. Arcones[1,2], and Y.-Z. Qian[3,4]
[1] Institut für Kernphysik, Technische Universität Darmstadt, Schlossgartenstr. 2, Darmstadt D-64289, Germany; julia.bliss@physik.tu-darmstadt.de
[2] GSI Helmholtzzentrum für Schwerionenforschung GmbH, Planckstr. 1, Darmstadt D-64291, Germany; almudena.arcones@physik.tu-darmstadt.de
[3] School of Physics and Astronomy, University of Minnesota, Minneapolis, MN 55455, USA; qian@physics.umn.edu
[4] Tsung-Dao Lee Institute, Shanghai 200240, People's Republic of China
Received 2018 April 11; revised 2018 August 26; accepted 2018 August 30; published 2018 October 17

Abstract

The origin of the so-called *p*-isotopes ^{92,94}Mo and ^{96,98}Ru in the solar system remains a mystery, as several astrophysical scenarios fail to account for them. In addition, data on presolar silicon carbide grains of type X (SiC X) exhibit peculiar Mo patterns, especially for ^{95,97}Mo. We examine the production of Mo and Ru isotopes in neutrino-driven winds associated with core-collapse supernovae (CCSNe) over a wide range of conditions. We find that proton-rich winds can make dominant contributions to the solar abundance of ^{98}Ru and significant contributions to those of ^{96}Ru, ^{92}Mo, and ^{94}Mo. In contrast, neutron-rich winds make negligible contributions to the solar abundances of ^{92,94}Mo and cannot produce ^{96,98}Ru, whereas the early ejecta of CCSNe can make dominant contributions to the solar abundance of ^{92}Mo. Furthermore, we show that some neutron-rich winds can account for the peculiar Mo patterns in SiC X grains. Our results can be generalized if conditions similar to those studied here are also obtained for other types of ejecta in either CCSNe or neutron star mergers.

Key words: nuclear reactions, nucleosynthesis, abundances – supernovae: general

1. Introduction

The isotopic abundances of the solar system obtained from meteoritic data (see, e.g., Lodders 2003) played a crucial role in establishing the framework of the basic processes of nucleosynthesis that gave rise to these abundances in particular and were responsible for the chemical evolution of the universe in general. For elements heavier than Fe, it is well known that the major sources for their solar abundances are the slow (*s*) and rapid (*r*) neutron-capture processes (Burbidge et al. 1957; Cameron 1957). In a number of cases, the most proton-rich isotopes of an element cannot be made by either of these processes and must be attributed to the so-called *p*-process (see, e.g., Meyer 1994; Arnould & Goriely 2003). There have been both observational and theoretical studies that strongly support low-mass ($\sim$1.5–3 $M_{\odot}$) stars during the asymptotic giant branch (AGB) stage of their evolution as the site for the main *s*-process producing Sr and heavier elements (see, e.g., Käppeler et al. 2011). It is also well known that massive ($>$10 $M_{\odot}$) stars during their pre-supernova evolution can produce nuclei up to ^{88}Sr through the weak *s*-process starting with the Fe in their birth material (see, e.g., Raiteri et al. 1993; Pignatari et al. 2010). The *p*-process is usually associated with (γ, *n*) reactions on the pre-existing nuclei as the shock propagates through the outer shells of a massive star during its supernova explosion (see Pignatari et al. 2016 for a review). A kilonova powered by the decay of newly synthesized *r*-process nuclei in a binary neutron star merger was observed recently (e.g., Kasen et al. 2017; Smartt et al. 2017). This observation demonstrates that mergers of two neutron stars or a neutron star and a black hole are important sites for the *r*-process (see, e.g., Freiburghaus et al. 1999b; Goriely et al. 2011; Korobkin et al. 2012). Other sites (see, e.g., Woosley & Hoffman 1992; Banerjee et al. 2011; Nishimura et al. 2015) associated with core-collapse supernovae (CCSNe) from massive stars have also been proposed and may play an important role in *r*-process enrichment at the earliest epochs (see, e.g., Qian & Wasserburg 2007; Hansen et al. 2014; Qian 2014).

In connection with modeling CCSNe (see, e.g., Janka 2012 for a review), new mechanisms for producing the elements from Zn to Ag with mass numbers $A \sim 64$–110 have been discovered (Woosley & Hoffman 1992; Hoffman et al. 1996; Fröhlich et al. 2006; Pruet et al. 2006). These are associated with neutrino-driven winds from the proto-neutron star created in a CCSN. Depending on the electron fraction, entropy, and expansion timescale (see, e.g., Qian & Woosley 1996), major production of some of the above elements occurs in the wind (see, e.g., Witti et al. 1994; Hoffman et al. 1997; Arcones & Montes 2011; Arcones & Bliss 2014). In these processes, (n, γ), (n, p), (p, γ), (α, γ), (α, n), (α, p), and their inverse reactions are all important (Woosley & Hoffman 1992; Bliss et al. 2017), in contrast to the dominance of neutron capture in both the *s*- and *r*-processes. For proton-rich winds, $\bar{\nu}_e + p \rightarrow n + e^+$ can provide neutrons to break through the bottleneck nuclei with slow β-decay by efficient (n, p) reactions. This νp-process (Fröhlich et al. 2006; Pruet et al. 2006; Wanajo 2006) can produce nuclei up to $A \sim 110$ and perhaps even further for the most favorable conditions.

As described above, a wide range of nuclei with $A \sim 64$–110 conventionally assigned to the *s*-, *r*-, and *p*-processes can be produced in neutrino-driven winds through very different mechanisms. The corresponding yield patterns are sensitive to the conditions in the wind (see, e.g., Arcones & Bliss 2014; Bliss et al. 2018) and usually distinct from the solar abundance pattern in this region. The isotopes ^{92,94}Mo and ^{96,98}Ru are commonly taken to be produced by the *p*-process only, but *p*-process models have difficulty in accounting for their solar abundances (see, e.g., Meyer 1994; Arnould & Goriely 2003). In this paper, we explore a wide range of wind conditions to study the production of Mo and Ru isotopes and the implications for the solar abundances of ^{92,94}Mo and ^{96,98}Ru. Further, in light of the

peculiar Mo patterns, especially for ^{95,97}Mo, and the associated anomalies in Zr found in presolar silicon carbide grains of type X (SiC X; Pellin et al. 1999, 2006), we also discuss possible nucleosynthetic contributions to these grains from neutrino-driven winds. Our results can be generalized if conditions similar to those explored here are also obtained for other types of ejecta in either CCSNe or neutron star mergers. Consequently, our study is complementary to post-processing studies based on specific simulations of these events.

2. Parametric Models of Neutrino-driven Winds

Nucleosynthesis in an expanding mass element starting from high temperature and density depends on the entropy S, expansion timescale τ, and electron fraction Y_e (Qian & Woosley 1996; Hoffman et al. 1997; Meyer & Brown 1997; Freiburghaus et al. 1999a; Otsuki et al. 2000; Thompson et al. 2001). One can study this nucleosynthesis in two complementary approaches: by analyzing Lagrangian tracer particles from hydrodynamical simulations or by means of a steady-state model (Otsuki et al. 2000; Thompson et al. 2001; Wanajo et al. 2001). While tracers from simulations allow us to study more realistic conditions, they have the disadvantage of being restricted to a limited number of available models. In contrast, steady-state models are ideal for studying a very broad set of conditions, even if some of those may not be realized in nature. Here we follow an intermediate approach. We take one tracer trajectory from a hydrodynamical simulation, specifically the trajectory ejected 8 s post-core bounce in model M15l1rl of Arcones et al. (2007), and parametrically vary its entropy and electron fraction. With this approach we aim to cover not only the conditions of one trajectory in one simulation, but to explore a broad range of conditions that can be realized in CCSNe when matter is ejected by neutrino heating. However, our approach cannot describe the early ejecta closely coupled to the dynamics of CCSN explosion even if we vary the nucleosynthesis parameters.

To calculate the nucleosynthesis, we use the same reaction network as in Fröhlich et al. (2006), which includes 4053 nuclei corresponding to the elements from H to Hf. The reaction rates are taken from JINA ReaclibV1.0 (Reaclib 2013), which is a compilation of theoretical rates from Rauscher & Thielemann (2000) and experimental rates from Angulo et al. (1999). The theoretical weak reaction rates in Fröhlich et al. (2006) are supplemented with experimental β-decay rates (NuDat2 2013) when available. The calculations start at $T(0) \sim 10$ GK, for which the composition is calculated from nuclear statistical equilibrium for a specific $Y_e(0)$. The subsequent evolution of the nuclear composition and Y_e is calculated using the full network that includes ν_e and $\bar{\nu}_e$ absorption on free neutrons and protons, respectively (Fröhlich et al. 2006). As described below, we always adjust the pertinent neutrino emission parameters so that they are consistent with the specified $Y_e(0)$ (Arcones & Bliss 2014).

We adopt the time evolution of the temperature $T(t)$ for the selected trajectory, which has an original entropy $S_0 = 85 k_B$/nuc (Boltzmann constant per nucleon). We change the entropy to $S = (0.5\text{–}1.5)S_0$ and obtain the new density evolution $\rho(t) = \rho_0(t) S_0/S$ assuming $S \propto T^3/\rho$, where $\rho_0(t)$ is the original density. For the electron fraction, we vary the initial value over the range $Y_e(0) = 0.45\text{–}0.62$. Further, we assume that $Y_e(0)$ is determined by the equilibrium between $\nu_e + n \rightarrow p + e^-$ and $\bar{\nu}_e + p \rightarrow n + e^+$ with an initial composition dominated by neutrons and protons and with negligible effects of electron and positron capture. Specifically,

$$Y_e(0) = \frac{1}{1 + \lambda_{\bar{\nu}_e p}(0)/\lambda_{\nu_e n}(0)}, \quad (1)$$

where $\lambda_{\bar{\nu}_e p}(0)$ and $\lambda_{\nu_e n}(0)$ are the initial rates for the reactions of concern. Note that

$$\lambda_{\nu_e n}(0) = \frac{L_{\nu_e}}{\langle E_{\nu_e}\rangle} \frac{\langle \sigma_{\nu_e n}\rangle}{4\pi r(0)^2}, \quad (2)$$

where L_{ν_e} and $\langle E_{\nu_e}\rangle$ are the (energy) luminosity and the average energy of ν_e, respectively, $\langle \sigma_{\nu_e n}\rangle$ is the average cross section, and $r(0)$ is the initial radius of the trajectory. A similar expression to Equation (2) applies to $\lambda_{\bar{\nu}_e p}(0)$. We assume the same number luminosity for ν_e and $\bar{\nu}_e$,

$$L_{\nu_e}/\langle E_{\nu_e}\rangle = L_{\bar{\nu}_e}/\langle E_{\bar{\nu}_e}\rangle, \quad (3)$$

and obtain

$$Y_e(0) = \frac{1}{1 + \langle \sigma_{\bar{\nu}_e p}\rangle/\langle \sigma_{\nu_e n}\rangle}. \quad (4)$$

We take the ν_e energy spectrum to be Fermi–Dirac with temperature T_{ν_e} and zero chemical potential, for which $\langle E_{\nu_e}\rangle = 3.15 T_{\nu_e}$, and similarly for $\bar{\nu}_e$. Under the above assumptions, $Y_e(0)$ only depends on T_{ν_e} and $T_{\bar{\nu}_e}$ through the average cross sections (see Equation (4)). For neutron-rich (proton-rich) winds, we fix $T_{\nu_e} = 5.32$ MeV ($T_{\bar{\nu}_e} = 6.35$ MeV) and choose $T_{\bar{\nu}_e}$ (T_{ν_e}) to match the $Y_e(0)$. To follow the subsequent evolution of Y_e, we need $\lambda_{\nu_e n}(t)$ and $\lambda_{\bar{\nu}_e p}(t)$. Using the time evolution $r(t)$ for the selected trajectory and the corresponding $L_{\nu_e} = 2.34 \times 10^{51}$ erg s^{-1} in the simulation of Arcones et al. (2007), we obtain

$$\lambda_{\nu_e n}(t) = \lambda_{\nu_e n}(0)[r(0)/r(t)]^2. \quad (5)$$

The rate $\lambda_{\bar{\nu}_e p}(t)$ is calculated similarly using $L_{\bar{\nu}_e} = L_{\nu_e} T_{\bar{\nu}_e}/T_{\nu_e}$ (see Equation (3)).

In principle, one can get the same $Y_e(0)$ for different combinations of ν_e and $\bar{\nu}_e$ luminosities and spectra. Different but reasonable neutrino emission parameters would change the nucleosynthesis yields somewhat for the same $Y_e(0)$ and S. In addition, the expansion timescale or, more generally, the expansion history has a significant impact on nucleosynthesis. For example, the presence of a reverse shock affects the expansion and the associated nucleosynthesis in proton-rich conditions (see Wanajo et al. 2011; Arcones et al. 2012). Whereas our parametric approach cannot cover all the possible variations of the input parameters, our study explores a wide range of conditions nonetheless. The results from our study should provide good guidance in finding the approximate conditions for producing the Mo and Ru isotopes of interest.

3. Results on Mo and Ru Isotopes

We are interested in the conditions under which various Mo and Ru isotopes can be made in environments similar to the neutrino-driven wind. In conventional terms, the seven stable isotopes of Mo (Ru) fall into four categories: (1) ^{92,94}Mo (^{96,98}Ru) as the p-only nuclei, (2) ^{96}Mo (^{100}Ru) as the s-only nuclide, (3) ^{95,97,98}Mo (^{99,101,102}Ru) as the mixed nuclei with contributions from the s- and r-processes, and (4) ^{100}Mo (^{104}Ru) as the r-only nuclide. As mentioned in the

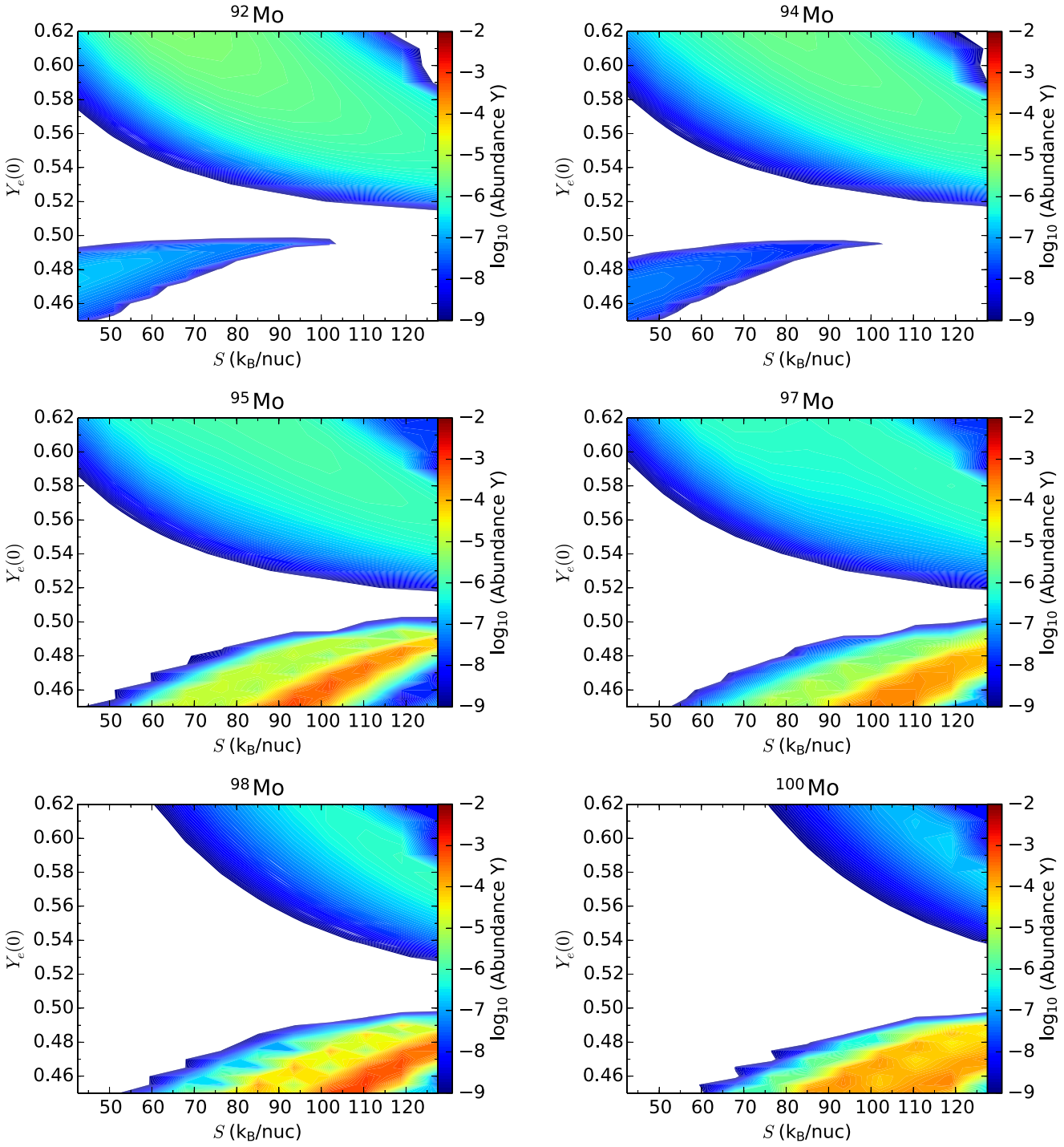

Figure 1. Color-coded contours illustrate the abundances (on a logarithmic scale) of the indicated Mo isotope produced for different $Y_e(0)$ and S. Abundances smaller than 10^{-9} are shown in white.

introduction, all these isotopes can be produced in the wind by processes that differ from the conventional *p*-, *s*-, and *r*-processes. However, for convenience, we will refer to these isotopes using the above conventional category labels.

We present in Figure 1 and Figure 2 the abundances of various Mo and Ru isotopes as functions of S and $Y_e(0)$. The behavior of the abundances is rather discontinuous in neutron-rich conditions, even for small variations of the input parameters. This behavior has been shown and discussed in Arcones & Montes (2011) and Arcones & Bliss (2014). Figure 1 shows that both the *p*-only nuclei ^{92,94}Mo can be produced in slightly neutron-rich [$Y_e(0) < 0.5$] or proton-rich [$Y_e(0) > 0.5$] winds for a significant range of S. In contrast, the *p*-only nuclei ^{96,98}Ru can be produced only in proton-rich winds but not in neutron-rich winds (see Figure 2).

Two distinct processes are responsible for producing ^{92,94}Mo in neutron- and proton-rich conditions, respectively. Neither of these processes is dominated by neutron capture. To reach ^{92,94}Mo in neutron-rich conditions, the nucleosynthesis path has to move along the valley of stability. If the neutron abundance is too large, the path goes further to the neutron-rich side and production of ^{92,94}Mo is blocked by ^{92,94}Zr, respectively. Therefore, production

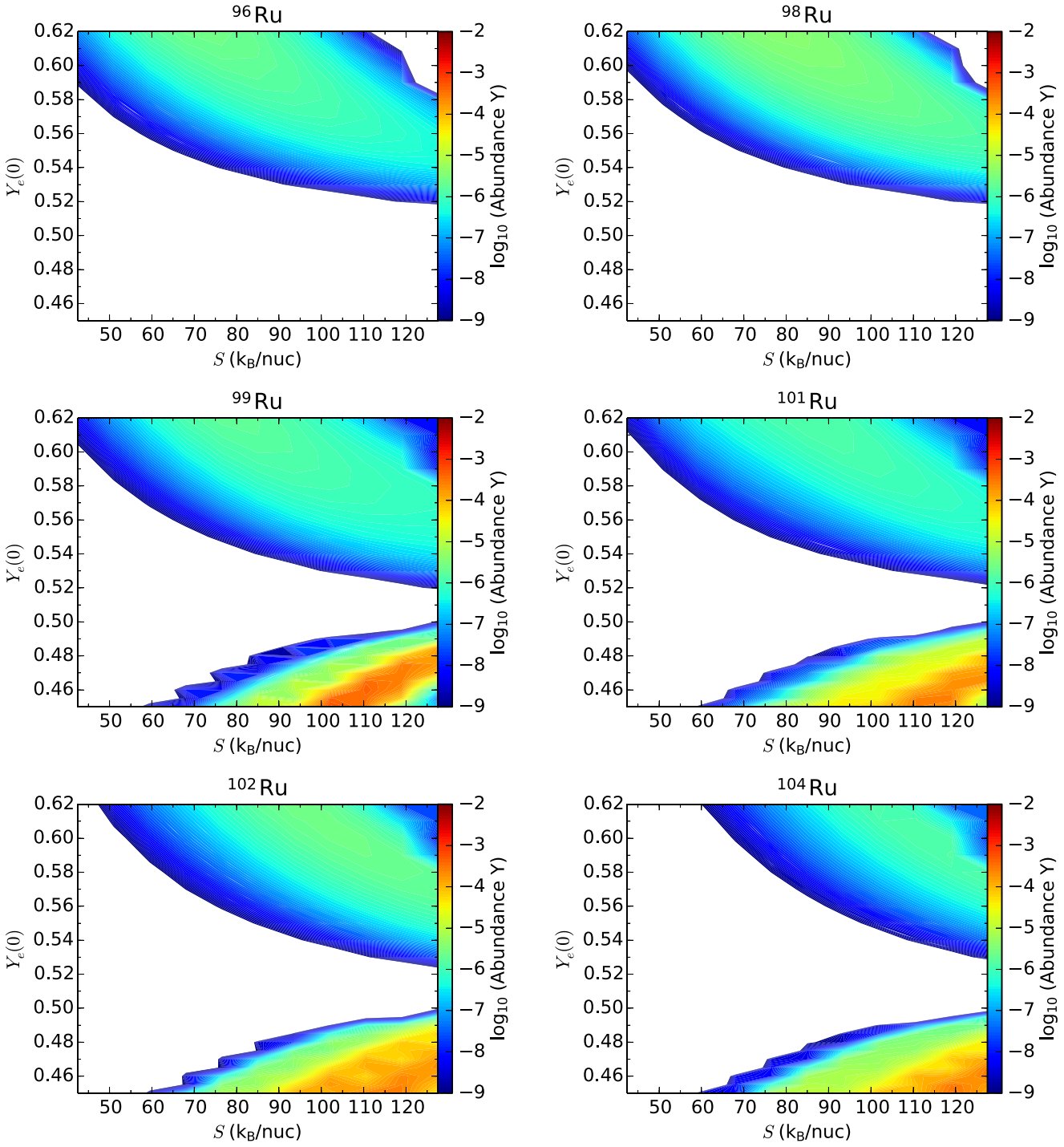

Figure 2. Same as Figure 1, but for Ru isotopes.

of ^{92,94}Mo requires that very few neutrons be present at freeze-out of charged-particle reactions with the composition dominated by α-particles and seed nuclei (see also Hoffman et al. 1996; Wanajo 2006; Farouqi et al. 2009). In addition to neutron capture, reactions involving light charged particles (e.g., protons and α-particles) play important roles in producing the seed nuclei including ^{92,94}Mo. Larger abundances of these two isotopes are obtained for smaller S, which favors a smaller number ratio of neutrons to the seed nuclei.

In proton-rich conditions, ^{92,94}Mo are produced by the νp-process, where (p, γ) and (n, p) reactions play key roles in driving the flow toward heavy nuclei. The (p, γ) reactions clearly depend on the proton abundance, and so do the (n, p) reactions with $\bar{\nu}_e + p \rightarrow n + e^+$ providing the neutrons. Because a larger $Y_e(0)$ and a higher S favor a higher proton abundance, the νp-process produces more ^{92,94}Mo with increasing $Y_e(0)$ and S initially (Pruet et al. 2006). However, when the number ratio of protons to the seed nuclei reaches a threshold, the abundances of ^{92,94}Mo start to decrease as the flow moves toward heavier nuclei.

The abundances of ^{92,94}Mo are rather low in neutron-rich conditions (see Figure 1). Because the nucleosynthesis path toward the p-only nuclei ^{96,98}Ru passes through ^{92,94}Mo, no significant amounts of ^{96,98}Ru can be synthesized in neutron-rich

conditions. In contrast, ^{96,98}Ru can be produced in proton-rich conditions similarly to ^{92,94}Mo (see Figure 2).

The mixed nuclei ^{95,97,98}Mo and ^{99,101,102}Ru, as well as the *r*-only nuclei ^{100}Mo and ^{104}Ru, are much more abundant in neutron-rich conditions (see Figures 1 and 2). Their production is due to neutron capture and generally increases for lower $Y_e(0)$ and higher S, which favor a higher ratio of neutrons to the seed nuclei. For typical neutron-rich conditions investigated here, the neutron-capture process stays close to the valley of stability on the neutron-rich side. Once the neutrons are consumed, β-decays populate ^{95,97,98,100}Mo and ^{99,101,102,104}Ru. For conditions giving rise to a high ratio of neutrons to the seed nuclei, the nucleosynthesis path moves farther away from stability and toward heavier nuclei, which leads to a decrease in production of Mo and Ru isotopes.

The *s*-only nuclei ^{96}Mo and ^{100}Ru can be synthesized only in proton-rich winds by late (n, γ) reactions (see Fröhlich et al. 2006; Wanajo 2006; Arcones et al. 2012). For this production channel to occur, a sufficient number of neutrons need to be available at the end of the νp-process. In any case, relative to the solar pattern of Mo (Ru) isotopes, the production of ^{96}Mo (^{100}Ru) is always much less significant than that of ^{92,94}Mo (^{96,98}Ru) for the conditions explored here (see, e.g., Figure 4).

3.1. Solar Abundances of ^{92,94}Mo and ^{96,98}Ru

Because our parametric study does not address the absolute amount of ejecta with a specific set of conditions, we cannot give the absolute nucleosynthetic yields for neutrino-driven winds. In any case, such yields must be combined with the frequency of occurrences for the corresponding conditions to provide the integrated production over the course of Galactic chemical evolution for comparison with the solar abundances. In view of the complications of Galactic chemical evolution, especially the substantial uncertainties in determining the amount of ejecta with a specific set of conditions in individual CCSNe, we do not attempt to estimate the integrated production by the winds from all the CCSNe that contributed to the solar abundances. Instead, we take the following simple approach to assess the possible contributions to the solar abundances of the *p*-isotopes ^{92,94}Mo and ^{96,98}Ru that these winds could have made. In order for an astrophysical environment to be a major source for the solar abundance of an isotope ^{i}E, a necessary condition is that this isotope must have a production factor $P(^i\mathrm{E})$ close to the maximum production factor $P_{\max}$ among all isotopes made in the same environment. The production factor $P(^i\mathrm{E})$ is defined as

$$P(^i\mathrm{E}) \equiv X(^i\mathrm{E})/X_\odot(^i\mathrm{E}), \quad (6)$$

where $X(^i\mathrm{E})$ and $X_\odot(^i\mathrm{E})$ are the mass fraction of the isotope ^{i}E produced in a model and observed in the solar system, respectively. The ratios $P(^i\mathrm{E})/P_{\max}$ for ^{92,94}Mo and ^{96,98}Ru are shown as color-coded contours for different S and $Y_e(0)$ in Figure 3.

It can be seen from Figure 3 that only ^{98}Ru can be produced with the maximum production factor in the wind. In fact, $P(^{98}\mathrm{Ru})/P_{\max} \sim 1$ is reached for a substantial range of conditions, e.g., $S \sim 60$–$120\ k_B$/nuc for $Y_e(0) \sim 0.54$–0.62. In contrast, the highest value of $P(^i\mathrm{E})/P_{\max}$ is ~0.35 (at $S \sim 59.5\ k_B$/nuc, $Y_e(0) \sim 0.61$) for ^{96}Ru, ~0.26 (at $S \sim 59.5\ k_B$/nuc, $Y_e(0) \sim 0.61$) for ^{92}Mo, and ~0.23 (at $S \sim 127.5\ k_B$/nuc, $Y_e(0) \sim 0.53$) for ^{94}Mo. These results suggest that proton-rich winds can make dominant contributions to the solar abundance of ^{98}Ru and significant contributions to those of ^{96}Ru ($\lesssim$35%), ^{92}Mo ($\lesssim$26%), and ^{94}Mo ($\lesssim$23%). Figure 3 also shows that neutron-rich winds make negligible contributions to the solar abundances of ^{92,94}Mo and cannot produce any significant amounts of ^{96,98}Ru.

The above results strongly suggest that sources other than the neutrino-driven wind, e.g., Type Ia supernovae (see Travaglio et al. 2014 for a recent study), are required to account for the solar abundances of ^{92,94}Mo and ^{96}Ru. While proton-rich winds can make dominant contributions to the solar abundance of ^{98}Ru, the exact contribution from this source can be determined only when contributions from other sources are established.

We emphasize that, in considering potential contributions from a source to the solar abundances of ^{92,94}Mo and ^{96,98}Ru, the associated $P(^i\mathrm{E})/P_{\max}$ values are a critical test. The production ratio of ^{92,94}Mo (^{96,98}Ru) relative to the solar value is secondary in that it is important only when the production factors for both isotopes are close to $P_{\max}$. Because only ^{98}Ru can have $P(^{98}\mathrm{Ru})/P_{\max} \sim 1$ in the wind, explanation of the ratios $(^{92}\mathrm{Mo}/^{94}\mathrm{Mo})_\odot = 1.60$ and $(^{96}\mathrm{Ru}/^{98}\mathrm{Ru})_\odot = 2.97$ (Lodders 2003) for the solar system crucially depends on other sources for these isotopes. In this regard, although both these ratios can be achieved in the wind (see Figure 3), this result is largely irrelevant for explaining the relative abundances of ^{92,94}Mo (^{96,98}Ru) in the solar system.

For illustration, we show in Figure 4 models that produce ^{92,94}Mo or ^{96,98}Ru in the solar ratio but have little to do with accounting for their abundance ratio in the solar system. The solar ratio for ^{92,94}Mo can be achieved in neutron-rich winds for $S = 60\ k_B$/nuc and $Y_e(0) = 0.475$ (top panel) or in proton-rich winds for $S = 120\ k_B$/nuc and $Y_e(0) = 0.54$ (middle panel). However, in neutron-rich winds, the predominantly produced isotopes are ^{88}Sr, ^{89}Y, and ^{90}Zr with the magic neutron number $N = 50$ (Witti et al. 1994; Hoffman et al. 1996, 1997), while the production factors for ^{92,94}Mo are only $\approx 2 \times 10^{-3} P_{\max}$. These production factors dramatically increase to $\approx 0.16 P_{\max}$ for proton-rich winds, but in this case ^{98}Ru has the largest production factor and ^{96}Ru is coproduced in a non-solar ratio. Nevertheless, this case represents approximately the optimal scenario for wind contributions to the solar abundances of ^{92,94}Mo and ^{96,98}Ru. Finally, the solar ratio for ^{96,98}Ru can be achieved in proton-rich winds for $S = 80\ k_B$/nuc and $Y_e(0) = 0.54$ (bottom panel). However, for these conditions the predominantly produced isotopes are ^{74}Se, ^{78}Kr, and ^{84}Sr.

Fisker et al. (2009) found that ^{92,94}Mo could be produced in the solar ratio in slightly proton-rich winds but with too small production factors to account for their solar abundances. Those results are qualitatively consistent with ours, although Fisker et al. used very different trajectories.

Hoffman et al. (1996) found that a neutrino-heated trajectory produces ^{70}Ge and the *p*-nuclei ^{74}Se, ^{78}Kr, ^{84}Sr, and ^{92}Mo in great abundance for $S = 49\ k_B$/nuc and $Y_e(0) = 0.485$ (see their Figure 2(b)). Wanajo et al. (2018) also found similar production in the innermost ejecta with similar conditions for their 27 $M_\odot$ CCSN model (see their Table 3 and Figure 14). We note that in both cases the material is ejected at <1 s post-core bounce and thus most affected by the dynamics of the explosion. The corresponding conditions cannot be adequately modeled by our parametric approach. The ejecta in both the above cases, however, produces very little ^{94}Mo and no ^{96,98}Ru,

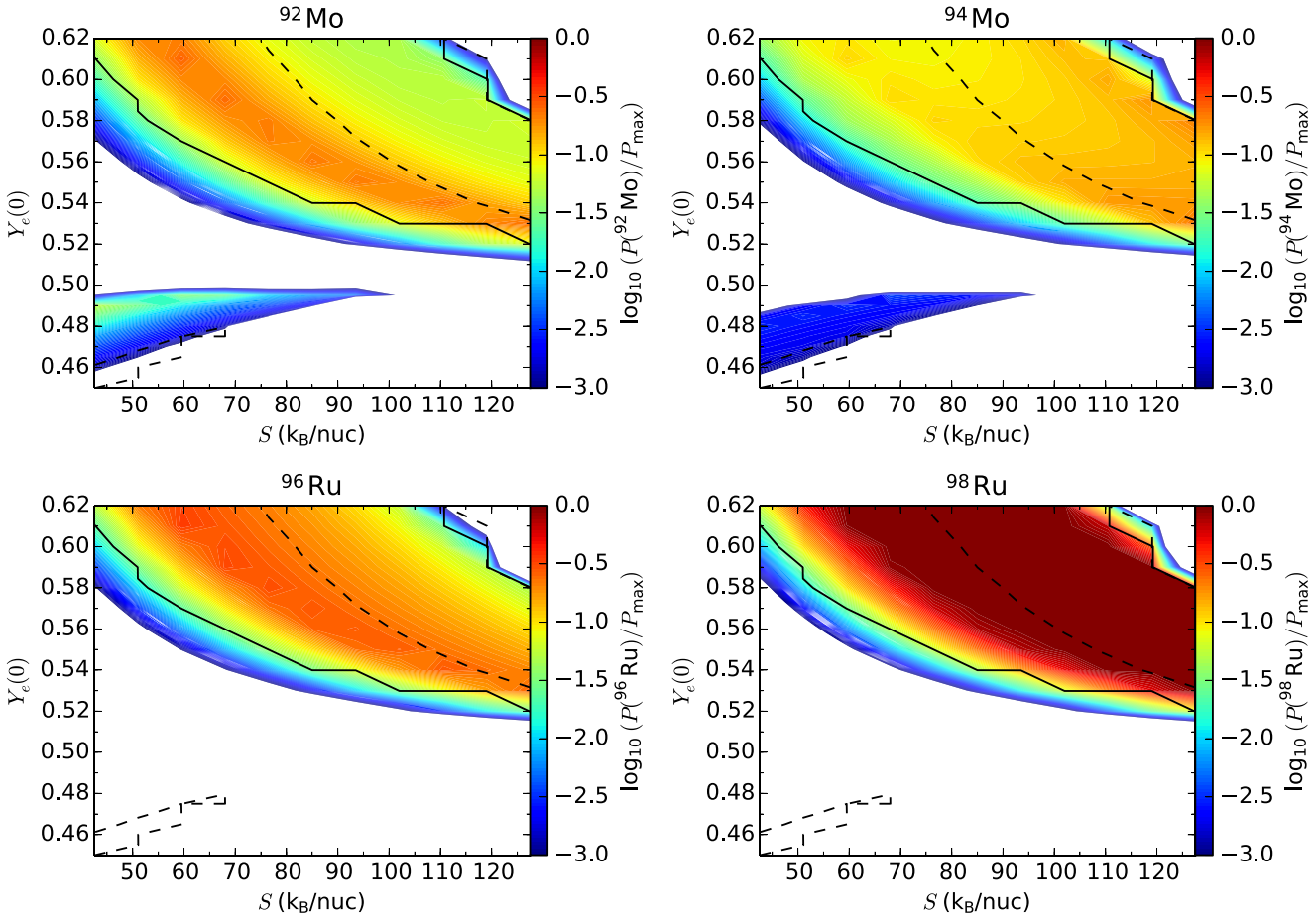

Figure 3. Color-coded contours illustrate the ratios (on a logarithmic scale) of the production factors of ^{92,94}Mo (upper panels) and ^{96,98}Ru (lower panels) relative to the maximum production factor among all isotopes produced for different $Y_e(0)$ and S. Ratios smaller than 10^{-3} are shown in white. For reference, the solid (dashed) curves correspond to conditions where the ratio $X(^{96}\mathrm{Ru})/X(^{98}\mathrm{Ru})$ [$X(^{92}\mathrm{Mo})/X(^{94}\mathrm{Mo})$] produced by the trajectory reaches the solar system value with the abundances of ^{96,98}Ru (^{92,94}Mo) exceeding 10^{-10}.

in qualitative agreement with our results for neutron-rich winds. Therefore, taking into account the early dynamical ejecta from CCSNe, which is not included in our parametric study, neutrino-heated ejecta from CCSNe can make dominant contributions to the solar abundance of ^{92}Mo in addition to that of ^{98}Ru, but other sources appear to be also required for explaining the solar abundances of ^{94}Mo and ^{96}Ru. Consequently, the solar ratios $(^{92}\mathrm{Mo}/^{94}\mathrm{Mo})_\odot$ and $(^{96}\mathrm{Ru}/^{98}\mathrm{Ru})_\odot$ are most likely produced by mixing contributions from different sources with non-solar ratios of these isotopes.

3.2. Peculiar Mo Patterns in SiC X Grains

Relative to ^{96}Mo, an *s*-only isotope, the *p*-only isotopes ^{92,94}Mo and the *r*-only isotope ^{100}Mo are nearly absent in mainstream SiC grains. This points to an *s*-process origin in AGB stars for the Mo patterns in such grains (see, e.g., Lugaro et al. 2003 for a detailed study). In contrast, SiC X grains have peculiar Mo patterns with large enrichments in the mixed isotopes ^{95,97}Mo (Pellin et al. 1999, 2006). Some of the X grains are also highly enriched in the *r*-only isotope ^{96}Zr (Davis et al. 1999; Pellin et al. 2006). While an *r*-process origin may account for the large enrichments in ^{96}Zr and ^{95,97}Mo, this is inconsistent with the data on the *r*-only isotope ^{100}Mo, which is not significantly enriched in most SiC X grains (Pellin et al. 1999, 2006).

Meyer et al. (2000) proposed to explain the overabundance of ^{95,97}Mo in SiC X grains with a neutron burst model (Howard et al. 1992). They first exposed a solar distribution of nuclei to a weak neutron fluence to mimic the weak *s*-process during the pre-supernova phase of a massive star (see e.g., Pignatari et al. 2010; Käppeler et al. 2011). Then they abruptly heated the processed matter to 1 GK to mimic the effect of a supernova shock and allowed the shocked matter to expand and cool. The burst of neutrons released by (α, n) reactions redistributed the initial abundances of Y and Zr isotopes to heavier isotopes up to $A \sim 97$, but the burst was not strong enough to accumulate much matter at ^{100}Zr. The original abundances of Mo isotopes were also redistributed to heavier isotopes. Finally, large abundances of ^{95,97}Mo were obtained upon the β decay of ^{95}Y and ^{95,97}Zr that were newly synthesized by the neutron burst.

While the above neutron burst model offers a potential explanation of the enrichments in ^{96}Zr and ^{95,97}Mo in SiC X grains, it remains to be seen if the conditions assumed could be provided by a detailed astrophysical model. Here we explore another potential explanation based on the neutrino-driven wind. Figure 5 shows the production factors for various isotopes made in the wind that corresponds to the trajectory with $S = 110\ k_B$/nuc and $Y_e(0) = 0.47$. It can be seen that ^{96}Zr

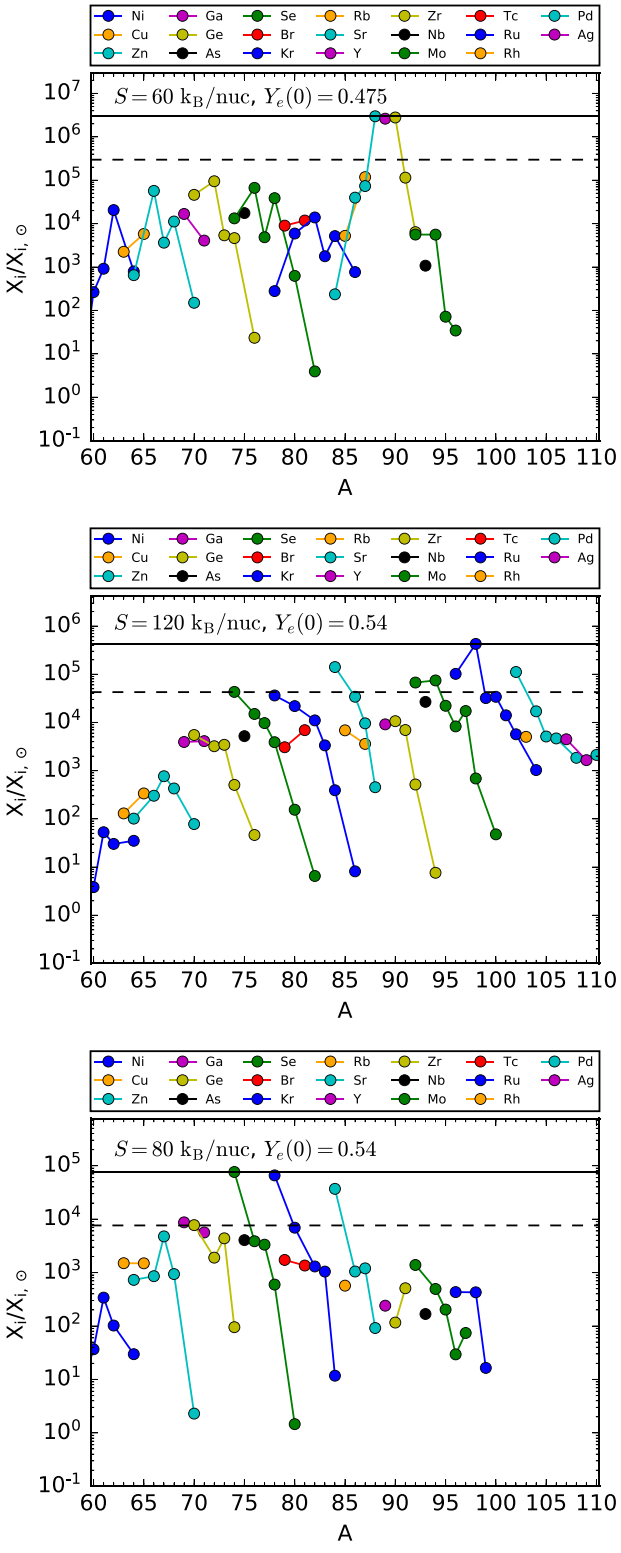

Figure 4. Ratio of the mass fraction of an isotope (X_i) relative to that observed in the solar system ($X_{i,\odot}$), i.e., the production factor, as a function of the mass number (A). Isotopes from the same element are connected by line segments. The horizontal lines indicate a normalization band given by the largest production factor (solid line) and a factor 10 less (dashed line). Nuclei falling within the band are the main products. The solar ratio of ^{92,94}Mo is achieved in the top and middle panels, while that of ^{96,98}Ru is achieved in the bottom panel. However, the actual ratio of ^{92,94}Mo and that of ^{96,98}Ru in the solar system must be explained by combining the wind and other sources.

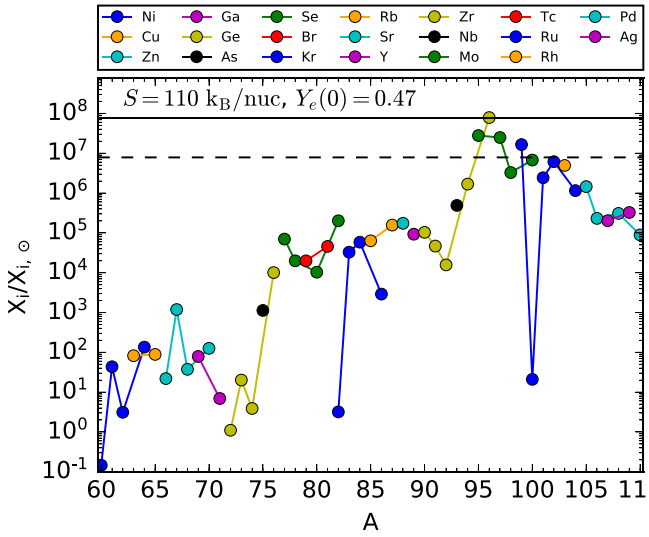

Figure 5. Same as Figure 4, but for wind conditions that are relevant for explaining the peculiar patterns of ^{95,97,98,100}Mo found in SiC X grains.

has the largest production factor and ^{95,97,98,100}Mo are also significantly produced. Further, the production factors for ^{95,97}Mo exceed those for ^{98,100}Mo, in agreement with the patterns in SiC X grains (Pellin et al. 1999, 2006). Specifically, the ratios of the production factors are $P(^{95}\text{Mo})$: $P(^{97}\text{Mo})$: $P(^{98}\text{Mo})$: $P(^{100}\text{Mo}) = 4.12$: 3.68: 0.49: 1. Note also that neither the p-only isotopes ^{92,94}Mo nor the s-only isotope ^{96}Mo is produced in this wind.

Because the sources for ^{92,94}Mo are uncertain, we focus on explaining the patterns of ^{95,96,97,98,100}Mo in SiC X grains. We consider that these five isotopes can be accounted for by mixtures of contributions from the s-process, the r-process, and the neutrino-driven wind. Specifically, we assign the s-only isotope ^{96}Mo exclusively to the s-process and use its abundance in a grain along with the solar s-process pattern to determine the s-process contributions to other Mo isotopes. Because the "r-only" isotope ^{100}Mo cannot be made in the s-process, we assign a fraction f_w of its abundance in a grain to the wind and the rest to the r-process. The r-process fraction $(1 - f_w)$ of the ^{100}Mo abundance in a grain is used along with the solar r-process pattern to determine the r-process contributions to other Mo isotopes. Consequently, the abundance of the isotope ^{i}Mo in a grain, $(^i\text{Mo})_g$, is given by

$$(^i\text{Mo})_g = \left(\frac{^i\text{Mo}}{^{96}\text{Mo}}\right)_s (^{96}\text{Mo})_g + \left[(1 - f_w)\left(\frac{^i\text{Mo}}{^{100}\text{Mo}}\right)_r + f_w\left(\frac{^i\text{Mo}}{^{100}\text{Mo}}\right)_w\right](^{100}\text{Mo})_g, \quad (7)$$

where the s-process, r-process, and wind production ratios $(^i\text{Mo}/^{96}\text{Mo})_s$, $(^i\text{Mo}/^{100}\text{Mo})_r$, and $(^i\text{Mo}/^{100}\text{Mo})_w$ are assumed to be fixed.

Equation (7) can be rewritten as

$$\frac{(^i\text{Mo}/^{96}\text{Mo})_g}{(^i\text{Mo}/^{96}\text{Mo})_\odot} = f_{s,\odot}(^i\text{Mo}) + \left[(1 - f_w)f_{r,\odot}(^i\text{Mo}) + f_w\frac{P(^i\text{Mo})}{P(^{100}\text{Mo})}\right]\frac{(^{100}\text{Mo}/^{96}\text{Mo})_g}{(^{100}\text{Mo}/^{96}\text{Mo})_\odot}, \quad (8)$$

where $f_{s,\odot}(^i\mathrm{Mo})$ and $f_{r,\odot}(^i\mathrm{Mo}) = 1 - f_{s,\odot}(^i\mathrm{Mo})$ are the s-process and r-process fractions of the solar ^{i}Mo abundance, respectively. We take $f_{s,\odot}(^i\mathrm{Mo}) = 0.50$, 0.59, 0.75, and 0 for ^{95}Mo, ^{97}Mo, ^{98}Mo, and ^{100}Mo, respectively. These values are consistent with both the estimates of Arlandini et al. (1999) and the s-process patterns found in mainstream SiC grains (e.g., Pellin et al. 1999). Note that the wind under discussion, with $S = 110\ k_\mathrm{B}$/nuc and $Y_e(0) = 0.47$, most likely occurs only rarely in CCSNe. This expectation is consistent with current CCSN models, which predict neutron-rich ejecta predominantly with $S < 50\ k_\mathrm{B}$/nuc (e.g., Wanajo et al. 2018), and with the observed rarity of SiC X grains, which represent just ~1% of the SiC grains (Pellin et al. 2006). Therefore, it is reasonable to assume $f_{r,\odot}(^i\mathrm{Mo}) = 1 - f_{s,\odot}(^i\mathrm{Mo})$ by ignoring the contributions from such winds to the solar abundances of the relevant Mo isotopes.

In terms of the meteoritic notation

$$\delta\ ^i\mathrm{Mo} \equiv 1000 \times \left[\frac{(^i\mathrm{Mo}/^{96}\mathrm{Mo})_g}{(^i\mathrm{Mo}/^{96}\mathrm{Mo})_\odot} - 1\right], \quad (9)$$

Equation (8) can be written as

$$\delta\ ^i\mathrm{Mo} = 10^3 f_w \left[\frac{P(^i\mathrm{Mo})}{P(^{100}\mathrm{Mo})} - f_{r,\odot}(^i\mathrm{Mo})\right] + \left[(1 - f_w) f_{r,\odot}(^i\mathrm{Mo}) + f_w \frac{P(^i\mathrm{Mo})}{P(^{100}\mathrm{Mo})}\right] \delta\ ^{100}\mathrm{Mo}. \quad (10)$$

Using the central value of $\delta\ ^{100}$Mo for a grain along with the wind production factor $P(^i\mathrm{Mo})$ relative to $P(^{100}\mathrm{Mo})$ and the solar r-process fraction $f_{r,\odot}(^i\mathrm{Mo})$ given above, we find f_w for which Equation (10) gives $\delta\ ^i$Mo in good agreement with the data on ^{95,97,98}Mo in the same grain. These results are shown in Figure 6 with $f_w = 0.11$, 0.14, 0.27, 0.19, and 0.39 for five SiC X grains, 113-2, 113-3, 209-1, 100-2, and B2-05 (Pellin et al. 2006), respectively. It can be seen that the above simple model including the wind contributions can explain the overall peculiar patterns of ^{95,97,98,100}Mo found in these grains. We expect that better agreement with the data, e.g., elimination of the discrepancy for ^{98}Mo in the grain 209-1, may be achieved by varying $\delta\ ^{100}$Mo within the measurement errors or using different wind conditions to optimize the wind production factors, or both. However, we consider that the results shown in Figure 6 are sufficient as a proof of concept.

The values of $f_w = 0.11$–0.39 used above to account for the overall patterns of ^{95,97,98,100}Mo in the five SiC X grains merit discussion. Based on their peculiar Mo patterns and other isotopic anomalies, these so-called presolar grains must have formed in individual stellar environments, most likely CCSNe, then migrated into the protosolar cloud, and finally survived the process of solar system formation (Pellin et al. 1999, 2006). As such, the peculiar isotopic pattern of a grain reflects the mixture of the newly synthesized yield pattern with the birth composition of the host CCSN. Whereas the mixing process is complicated, it is reasonable that the contribution of ^{100}Mo from the host CCSN to the grain, as indicated by f_w, can be substantial although, as mentioned above, such CCSNe made negligible contributions to the solar abundances of this and other Mo isotopes. Furthermore, if the major sources for the p-isotopes ^{92,94}Mo are decoupled from the r-process source for ^{100}Mo, then the birth material of the host CCSNe for different grains may have had close to solar abundances of ^{92,94}Mo but very different abundances of ^{100}Mo. We propose that the Mo isotopes in SiC X grains reflect only mixtures of the rare neutron-rich wind invoked above, which cannot produce ^{92,94}Mo, with the birth

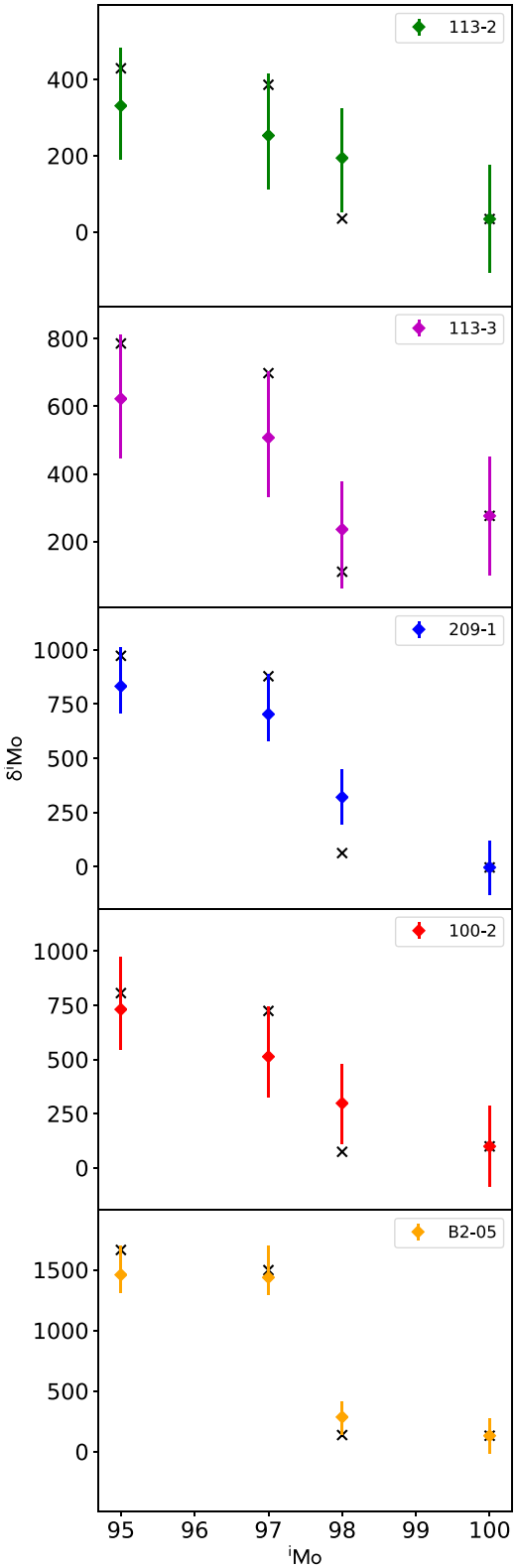

Figure 6. Comparison of the model (crosses) including wind contributions and the data (colored diamonds with error bars) on the peculiar patterns of ^{95,97,98,100}Mo in five SiC X grains (Pellin et al. 2006).

material of the host CCSNe, which had close to solar abundances of these two isotopes but widely varying abundances of ^{100}Mo. This scenario may explain why SiC X grains are not very anomalous in ^{92,94}Mo (Pellin et al. 1999, 2006).

4. Conclusions

We have conducted a detailed parametric study on the production of Mo and Ru isotopes in neutrino-driven winds. Although we have only presented results based on the trajectory ejected 8 s post-core bounce in the CCSN simulation of Arcones et al. (2007) by varying the entropy and the initial Y_e, we have also studied similar models based on other trajectories ejected at >1 s post-core bounce and found similar trends for nucleosynthesis. With regard to the *p*-isotopes, we find that proton-rich winds can make dominant contributions to the solar abundance of ^{98}Ru and significant contributions to those of ^{96}Ru, ^{92}Mo, and ^{94}Mo. In contrast, neutron-rich winds described by our parametric model make negligible contributions to the solar abundances of ^{92,94}Mo and cannot produce ^{96,98}Ru. However, we have shown that some neutron-rich winds can account for the peculiar patterns of ^{95,97,98,100}Mo in SiC X grains. Our results can be generalized if conditions similar to those studied here are also obtained for other types of ejecta in either CCSNe or neutron star mergers. Consequently, our study is complementary to post-processing studies based on specific simulations of these events.

Our parametric model cannot adequately describe the neutrino-heated ejecta at <1 s post-core bounce that is closely coupled to the dynamics of CCSN explosion. Hoffman et al. (1996) and Wanajo et al. (2018) showed that such early neutron-rich ejecta may account for the solar abundance of ^{92}Mo. Taking both their results and ours into account, we conclude that neutrino-heated ejecta from CCSNe can make dominant contributions to the solar abundances of ^{92}Mo and ^{98}Ru, but other sources are also required to account for those of ^{94}Mo and ^{96}Ru. Finally, only a detailed study of integrated production by all the sources can address quantitatively how the solar abundances of the *p*-isotopes ^{92,94}Mo and ^{96,98}Ru were obtained through the course of Galactic chemical evolution.

We acknowledge useful discussions with Camilla J. Hansen, Maria Lugaro, Marco Pignatari, and Claudia Travaglio. We thank an anonymous referee for a detailed and constructive report that helped improve the paper. This work was supported in part by the Helmholtz-University Young Investigator grant No. VH-NG-825, Deutsche Forschungsgemeinschaft through SFB 1245, BMBF under grant No. 05P15RDFN1, ERC 677912 EUROPIUM, and the US DOE grant DE-FG02-87ER40328.

ORCID iDs

Y.-Z. Qian https://orcid.org/0000-0002-3146-2668

References

Angulo, C., Arnould, M., Rayet, M., et al. 1999, NuPhA, 656, 3
Arcones, A., & Bliss, J. 2014, JPhG, 41, 044005
Arcones, A., Fröhlich, C., & Martínez-Pinedo, G. 2012, ApJ, 750, 18
Arcones, A., Janka, H.-T., & Scheck, L. 2007, A&A, 467, 1227
Arcones, A., & Montes, F. 2011, ApJ, 731, 5
Arlandini, C., Käppeler, F., Wisshak, K., et al. 1999, ApJ, 525, 886
Arnould, M., & Goriely, S. 2003, PhR, 384, 1
Banerjee, P., Haxton, W. C., & Qian, Y.-Z. 2011, PhRvL, 106, 201104
Bliss, J., Arcones, A., Montes, F., & Pereira, J. 2017, JPhG, 44, 054003
Bliss, J., Witt, M., Arcones, A., Montes, F., & Pereira, J. 2018, ApJ, 855, 135
Burbidge, E. M., Burbidge, G. R., Fowler, W. A., & Hoyle, F. 1957, RvMP, 29, 547
Cameron, A. G. W. 1957, AJ, 62, 9
Davis, A. M., Pellin, M. J., Lewis, R. S., Amari, S., & Clayton, R. N. 1999, Meteoritics & Planet. Sci. Suppl., 34, 30
Farouqi, K., Kratz, K.-L., Mashonkina, L. I., et al. 2009, ApJL, 694, L49
Fisker, J. L., Hoffman, R. D., & Pruet, J. 2009, ApJL, 690, L135
Freiburghaus, C., Rembges, J.-F., Rauscher, T., et al. 1999a, ApJ, 516, 381
Freiburghaus, C., Rosswog, S., & Thielemann, F.-K. 1999b, ApJL, 525, L121
Fröhlich, C., Martínez-Pinedo, G., Liebendörfer, M., et al. 2006, PhRvL, 96, 142502
Goriely, S., Bauswein, A., & Janka, H.-T. 2011, ApJL, 738, L32
Hansen, C. J., Montes, F., & Arcones, A. 2014, ApJ, 797, 123
Hoffman, R. D., Woosley, S. E., Fuller, G. M., & Meyer, B. S. 1996, ApJ, 460, 478
Hoffman, R. D., Woosley, S. E., & Qian, Y.-Z. 1997, ApJ, 482, 951
Howard, W. M., Meyer, B. S., & Clayton, D. D. 1992, Metic, 27, 404
Janka, H.-T. 2012, ARNPS, 62, 407
Käppeler, F., Gallino, R., Bisterzo, S., & Aoki, W. 2011, RvMP, 83, 157
Kasen, D., Metzger, B., Barnes, J., Quataert, E., & Ramirez-Ruiz, E. 2017, Natur, 551, 80
Korobkin, O., Rosswog, S., Arcones, A., & Winteler, C. 2012, MNRAS, 426, 1940
Lodders, K. 2003, ApJ, 591, 1220
Lugaro, M., Davis, A. M., Gallino, R., et al. 2003, ApJ, 593, 486
Meyer, B. S. 1994, ARA&A, 32, 153
Meyer, B. S., & Brown, J. S. 1997, ApJS, 112, 199
Meyer, B. S., Clayton, D. D., & The, L.-S. 2000, ApJL, 540, L49
Nishimura, N., Takiwaki, T., & Thielemann, F.-K. 2015, ApJ, 810, 109
NuDat2 2013, National Nuclear Data Center, Information Extracted from the NuDat 2 Database, http://www.nndc.bnl.gov/nudat2/
Otsuki, K., Tagoshi, H., Kajino, T., & Wanajo, S. 2000, ApJ, 533, 424
Pellin, M. J., Davis, A. M., Lewis, R. S., Amari, S., & Clayton, R. N. 1999, LPSC, 30, 1969
Pellin, M. J., Savina, M. R., Calaway, W. F., et al. 2006, LPSC, 37, 2041
Pignatari, M., Gallino, R., Heil, M., et al. 2010, ApJ, 710, 1557
Pignatari, M., Göbel, K., Reifarth, R., & Travaglio, C. 2016, IJMPE, 25, 1630003
Pruet, J., Hoffman, R. D., Woosley, S. E., Janka, H.-T., & Buras, R. 2006, ApJ, 644, 1028
Qian, Y.-Z. 2014, JPhG, 41, 044002
Qian, Y.-Z., & Wasserburg, G. J. 2007, PhR, 442, 237
Qian, Y.-Z., & Woosley, S. E. 1996, ApJ, 471, 331
Raiteri, C. M., Gallino, R., Busso, M., Neuberger, D., & Kaeppeler, F. 1993, ApJ, 419, 207
Rauscher, T., & Thielemann, F.-K. 2000, ADNDT, 75, 1
Reaclib 2013, Database of Joint Institute of Nuclear Astrophysics, http://www.jinaweb.org
Smartt, S. J., Chen, T.-W., Jerkstrand, A., et al. 2017, Natur, 551, 75
Thompson, T. A., Burrows, A., & Meyer, B. S. 2001, ApJ, 562, 887
Travaglio, C., Gallino, R., Rauscher, T., et al. 2014, ApJ, 795, 141
Wanajo, S. 2006, ApJ, 647, 1323
Wanajo, S., Janka, H.-T., & Kubono, S. 2011, ApJ, 729, 46
Wanajo, S., Kajino, T., Mathews, G. J., & Otsuki, K. 2001, ApJ, 554, 578
Wanajo, S., Müller, B., Janka, H.-T., & Heger, A. 2018, ApJ, 852, 40
Witti, J., Janka, H.-T., & Takahashi, K. 1994, A&A, 286, 841
Woosley, S. E., & Hoffman, R. D. 1992, ApJ, 395, 202